Journal of Nonlinear Evolution Equations and Applications ISSN 2161-3680
Volume 2016, Number 1, pp. 1–23 (August 2016) http://www.jneea.com

NUMERICAL STUDY OF TRANSIENT HYDROMAGNETIC FORCED CONVECTIVE SLIP FLOW OVER A POROUS ROTATING DISK WITH THERMOPHORESIS

M. S. Alam, M. Mahabubur Rahman
Department of Mathematics, Jagannath University, Dhaka-1100, Bangladesh

M. M. Rahman*, M. J. Uddin
Department of Mathematics and Statistics, College of Science, Sultan Qaboos University
P.O. Box 36, P.C. 123, Al-Khod, Muscat, Sultanate of Oman

K. Vajravelu
Department of Mathematics, University of Central Florida, Orlando, FL 32816, USA

Received on October 3, 2015
Revised version on November 10, 2015
Accepted on November 4, 2015 (with modifications), December 2015 (final version)

Communicated by Joydev Chattopadhyay

Abstract. This paper deals with the problem of unsteady, laminar forced convective heat and mass transfer flow of a viscous incompressible fluid with thermophoresis due to a porous rotating disk in the presence of partial slip and magnetic field. The numerical simulation is carried out for the solution of nonlinear partial differential equations by applying Nachtsheim–Swigert shooting iteration technique along with sixth-order Runge–Kutta iteration scheme. Comparison with previously published work for the steady case is performed and results are found to be in excellent agreement. The effects of the model parameters on the dimensionless velocity (radial, tangential and axial), temperature, and concentration fields are displayed graphically. The local skin-friction coefficient (radial and tangential) and the local Nusselt number are also calculated and tabulated. The obtained results show that the axial thermophoretic velocity is increased with the increasing values of the thermophoretic coefficient and the thermophoresis parameter. The results also show that the applied magnetic field and the slip parameter strongly control the flow, heat and mass transfer characteristics.

Keywords: Boundary layer, hydromagnetic slip flow, rotating disk, thermophoresis.

2010 Mathematics Subject Classification: 76D05, 76E06, 76N20, 76R05.

*e-mail address: mansurdu@yahoo.com, mansur@squ.edu.om; fax: +968 2414 1490

1 Introduction

Thermophoresis, the motion of suspended particles in a fluid induced by a temperature gradient, is of practical importance in a variety of industrial and engineering applications including aerosol collection (thermal precipitators), nuclear reactor safety, gas cleaning, corrosion of heat exchangers, and micro contamination control. Thermophoresis phenomenon is observed when mixtures of two or more types of movable particles (particles able to move) are subjected to the temperature gradient and the different types of particles respond differently. A common example that may be observed by the naked eye with good lighting is when the hot rod of an electric heater is surrounded by tobacco smoke: the smoke goes away from the immediate vicinity of the hot rod. As the small particles of air nearest the hot rod are heated, they create a fast flow away from the rod, in the direction of decreasing temperature. They have acquired higher kinetic energy with their higher temperature. When they collide with the large, slower-moving particles of the tobacco smoke they push the latter away from the rod. The force that has pushed the smoke particles away from the rod is an example of a thermophoretic force. So, the velocity acquired by the particles is called the thermophoretic velocity and the force experienced by the suspended particles due to the temperature gradient is known as the thermophoretic force.

Thermophoresis in laminar flow over a horizontal flat plate has been studied theoretically by Goren [19]. He observed that the deposition on cold plate and particle free layer thickness in hot plate case. Talbot et al. [43] analyzed the effects of thermophoresis of particles in a heated boundary layer. Mills et al. [27] studied thermophoresis on aerosol particle deposition. They also observed this phenomenon in laminar boundary layer on a flat plate. Thermophoresis in a free convection flow on a cold vertical flat surface was analyzed by Epstein et al. [15]. Garg and Jayaraj [17] studied the numerical calculation for thermophoretic deposition of a laminar slot jet on an inclined plate. In their analysis they used hot, cold and adiabatic wall. The thermophoretic transport of aerosol particles through a forced convection laminar boundary layer in cross flow over a cylinder was studied by Garg and Jayaraj [18]. Jia et al. [23] investigated numerically the interaction between radiation and thermophoresis in forced convection laminar boundary layer flow. The effect of the thermophoresis on submicron particle deposition from a laminar forced convection boundary layer over an isothermal cylinder was investigated by Chiou and Cleaver [10] whereas Chiou [11] analyzed the effect of thermophoresis on submicron particle deposition from a forced convective boundary layer flow on to an isothermal moving plate through similarity analysis. Thermophoresis in natural convection with variable properties for a laminar flow over a cold vertical flat plate has been studied by Jayaraj et al. [22]. Tsai [44] found an approach for determining the influence of suction in the wall and thermophoresis on an aerosol particle deposition. For a cold plate he noticed that concentration of the particles at the wall increases with the decrease of the Prandtl number. The problem of steady, two-dimensional, laminar, hydrodynamic flow with heat and mass transfer over a semi-infinite permeable flat surface in the presence of the thermophoresis and heat generation was studied by Chamkha and Issa [8]. In their analysis, they found that as the thermophoretic parameter increases, the surface mass flux increases. Chamkha et al. [9] studied the effect of thermophoresis particle deposition in free convection boundary layer from a vertical flat plate embedded in a porous medium. Their numerical results showed that the mean deposition effect of the wavy plate is greater than the plate. Mixed convection heat and mass transfer flow along an isothermal vertical flat plate embedded in a fluid-saturated porous medium and the effects of viscous dissipation and thermophoresis in both aiding and opposing flows studied by Seddeek [41]. The effect of thermophoresis particle deposition in a free convection boundary layer flow over a horizontal flat plate embedded in a porous medium was studied by Postelnicu [31]. Bakier and Mansour [5] studied numerically the combined effects

of magnetic field and thermophoresis particle deposition in free convection boundary layer along a vertical flat plate embedded in a porous medium. Duwairi and Damesh [14] analyzed the effects of thermophoresis particle deposition on mixed convection flow along a vertical surface placed in a porous medium. Damesh et al. [13] studied non-similar solution of magnetohydrodynamic and thermophoretic particle deposition on mixed convection problem in a porous medium along a vertical surface with variable wall temperature. Having practical importance of thermophoresis phenomenon Alam et al. [2] studied thermophoretic particle deposition on two-dimensional hydromagnetic heat and mass transfer flow over an inclined flat plate with various flow conditions. Rahman and Postelnicu [34] studied the effect of thermophoresis on steady forced convective laminar flow of a viscous incompressible fluid over a rotating disk. Rahman et al. [33] studied the thermophoresis particle deposition on unsteady two-dimensional forced convective heat and mass transfer flow along a wedge with variable viscosity and variable Prandtl number whereas Postelnicu [32] studied the thermophoresis particle deposition in natural convection over inclined surface in porous medium.

Rotating disk flows along with heat transfer is one of the classical problems of fluid mechanics, which has both theoretical and practical values. Flow due to a rotating disk is encountered in many industrial devices, geothermal and geophysical systems. The importance of heat transfer from a rotating body can be found in various types of machinery, for example computer disk drives and gas turbine rotors. The first solution to the classical problem of rotating disk flow was obtained by Karman [24]. The results of Karman [24] were further improved by Cochran [12]. Bödewadt [7] studied the flow over a stationary disk and the fluid at infinity rotates with a uniform angular velocity. He noticed that suction essentially decreases both the radial and tangential components of the velocity but increases the axial flow towards the disk at infinity. Wagner [45], and Millsaps and Pohlhausen [28] found that the heat transfer from a disk having uniform surface temperature was different from that of the isothermal surroundings. Maleque and Sattar [25] investigated the influence of variable properties on the physical quantities of the rotating disk problem by obtaining a self-similar solution of the Navier-Stokes equations along with the energy equation. Attia [4] investigated the steady flow and heat transfer over a rotating disk in a porous medium. Zueco and Rubio [47] analyzed the network method to study magnetohydrodynamic flow and heat transfer over a rotating disk.

The no-slip boundary condition is known as the main manifestation of the Navier-Stokes theory of fluid dynamics. In certain situations, the assumption of no-slip boundary condition does no longer apply. When fluid flows in micro electrical mechanical systems (MEMS), the no-slip condition at the solid fluid interface is no longer applicable. A slip flow model more accurately describes the non-equilibrium near the interface. A partial slip may occur on a stationary and moving boundary when the fluid is particulate such as emulsions, suspensions, foams, and polymer solutions. Sparrow et al. [42] studied the flow of Newtonian fluid due to the rotation of a porous-surfaced disk with a set of linear slip-flow conditions. A substantial reduction in torque then occurred as a result of surface slip. Miklavčič and Wang [26] further revisited the problem of Sparrow et al. [42] and pointed out that the slip flow boundary conditions could also be used for slightly rarefied gases or for flow over grooved surfaces. Arikoglu and Ozkol [3] studied MHD slip flow over a rotating disk with heat transfer. It is observed that both the slip factor and the magnetic flux decreases the velocity in all directions and thicken the thermal boundary layer. Osalusi et al. [30] studied thermal-diffusion and diffusion-thermo effects on MHD slip flow due to a rotating disk. Rahman and Sattar [37] and Rahman [36, 38] studied thermophoretic particle deposition over a rapidly rotating permeable disk with variable fluid properties in the presence of partial slip, magnetic field, thermal-diffusion and diffusion-thermo effects. Also, the effects of magnetic field and slip parameter can be found in the notable works of Rahman and Eltayeb [35], Hakeem et al. [20, 21] and Ganga et al. [16].

The objective of the present paper is to investigate the effects of thermophoresis on unsteady hydromagnetic forced convective heat and mass transfer flow over a cold rapidly rotating permeable disk in the presence of partial slip and magnetic field. Using similarity transformations, the governing equations for flow, heat and mass transfer have been transformed into a system of ordinary differential equations which are then solved numerically applying Nachtsheim–Swigert shooting iteration technique with sixth-order Runge–Kutta integration scheme. To the best of the author's knowledge no research has come out considering the above-stated model and flow conditions.

2 Governing equations of the flow

In a non-rotating cylindrical polar frame of reference (r, φ, z), where z is the vertical axis in the cylindrical coordinates system with r and φ as the radial and tangential axes respectively, let us consider a disk which rotates with constant angular velocity Ω about the z axis. The disk is placed at $z = 0$, and a viscous incompressible Newtonian and electrically conducting fluid occupies the region $z > 0$. An external uniform magnetic field is applied perpendicular to the surface (*i.e.* in the z direction) of the disk and has a constant magnetic flux density (or, applied magnetic field) B_0 everywhere in the fluid. The assumption is valid only when the magnetic Reynolds number is very small. A uniform suction or injection through the disk is considered. The flow configurations and geometrical coordinates are shown in Fig. 1. The components of the flow velocity q are (u, v, w) in

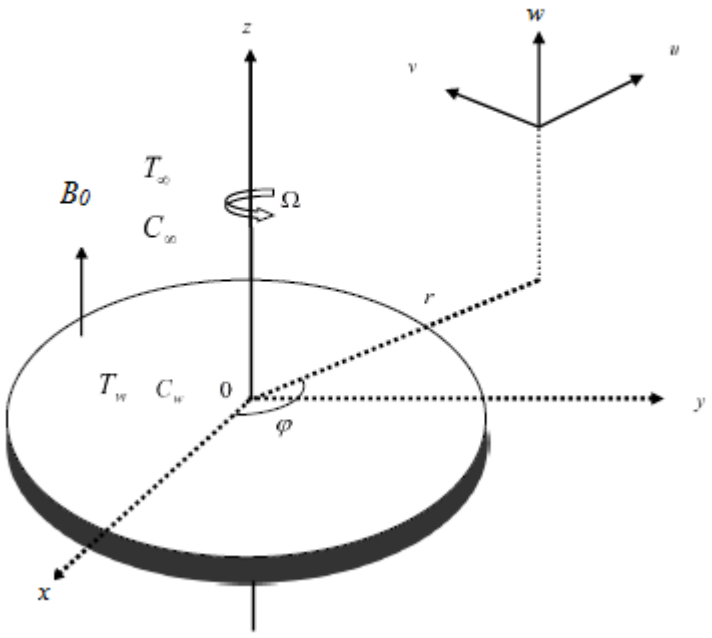

Figure 1: Flow configurations and coordinate system.

the direction of increasing (r, φ, z) respectively. The surface of the rotating disk is maintained at a uniform temperature T_w and far away from the wall, the free stream temperature is T_∞ ($T_\infty > T_w$). The species concentration at the surface is maintained uniform at C_w, which is taken to be zero

and that of the ambient fluid is assumed to be C_∞. At $t < 0$ the fluid is at rest and at constant temperature and concentration and the disk does not rotate. At $t = 0$ the disk is instantaneously put into a motion (impulsively accelerated) at constant angular velocity. Only because of this the flow is actually transient during a very small time interval before reaching to the well-known steady-state. The effects of thermophoresis are being taken into account to help in the understanding of the mass deposition variation on the surface. We further assume that (i) the mass flux of particles is sufficiently small so that the main stream velocity and temperature fields are not affected by the thermo physical processes experienced by the relatively small number of particles, (ii) when particles hit the disk surface, they will be absorbed by it and none will be bounced back, (iii) due to the boundary layer behavior the temperature gradient in the z direction is much larger than that in the r direction and hence only the thermophoretic velocity component which is normal to the surface is of importance, (iv) the fluid has constant kinematic viscosity and thermal diffusivity, (v) the particle diffusivity is assumed to be constant, and the concentration of particles is sufficiently dilute to assume that particle coagulation in the boundary layer is negligible and (vi) the flow is unsteady and axially symmetric.

Under the above-stated assumptions, the continuity, momentum, energy and particle concentration equations can be written as (see also Rahman and Postelnicu [34]):

$$\frac{\partial u}{\partial r} + \frac{u}{r} + \frac{\partial w}{\partial z} = 0, \tag{2.1}$$

$$\frac{\partial u}{\partial t} + u\frac{\partial u}{\partial r} - \frac{v^2}{r} + w\frac{\partial u}{\partial z} = -\frac{1}{\rho}\frac{\partial p}{\partial r} + \nu\left(\frac{\partial^2 u}{\partial r^2} + \frac{1}{r}\frac{\partial u}{\partial r} - \frac{u}{r^2} + \frac{\partial^2 u}{\partial z^2}\right) - \frac{\sigma B_0^2}{\rho}u, \tag{2.2}$$

$$\frac{\partial v}{\partial t} + u\frac{\partial v}{\partial r} + \frac{uv}{r} + w\frac{\partial v}{\partial z} = \nu\left(\frac{\partial^2 v}{\partial r^2} + \frac{1}{r}\frac{\partial v}{\partial r} - \frac{v}{r^2} + \frac{\partial^2 v}{\partial z^2}\right) - \frac{\sigma B_0^2}{\rho}v, \tag{2.3}$$

$$\frac{\partial w}{\partial t} + u\frac{\partial w}{\partial r} + w\frac{\partial w}{\partial z} = -\frac{1}{\rho}\frac{\partial p}{\partial z} + \nu\left(\frac{\partial^2 w}{\partial r^2} + \frac{1}{r}\frac{\partial w}{\partial r} + \frac{\partial^2 w}{\partial z^2}\right), \tag{2.4}$$

$$\frac{\partial T}{\partial t} + u\frac{\partial T}{\partial r} + w\frac{\partial T}{\partial z} = \alpha\left(\frac{\partial^2 T}{\partial r^2} + \frac{1}{r}\frac{\partial T}{\partial r} + \frac{\partial^2 T}{\partial z^2}\right), \tag{2.5}$$

$$\frac{\partial C}{\partial t} + u\frac{\partial C}{\partial r} + w\frac{\partial C}{\partial z} = D\left(\frac{\partial^2 C}{\partial r^2} + \frac{1}{r}\frac{\partial C}{\partial r} + \frac{\partial^2 C}{\partial z^2}\right) - \frac{\partial}{\partial r}(U_T C) - \frac{\partial}{\partial z}(W_T C), \tag{2.6}$$

where the variables and related quantities are defined in the nomenclature. The thermophoretic velocities U_T and W_T which appear in equation (2.6), can be written as (see also Rahman and Postelnicu [34])

$$U_T = -\frac{\kappa\nu}{T}\frac{\partial T}{\partial r}, \;\; W_T = -\frac{\kappa\nu}{T}\frac{\partial T}{\partial z}, \tag{2.7}$$

where κ is the thermophoretic coefficient which ranges in value from 0.2 to 1.2 as indicated by Batchelor and Shen [6] and is defined from the theory of Talbot et al. [43] by

$$\kappa = \frac{2C_s(\lambda_g/\lambda_p + C_t Kn)[1 + Kn(C_1 + C_2 e^{-C3/Kn})]}{(1 + 3C_m Kn)(1 + 2\lambda_g/\lambda_p + 2C_t Kn)}, \tag{2.8}$$

where C_1, C_2, C_3, C_m, C_s, C_t are constants, λ_g and λ_p are the thermal conductivities of the fluid and diffused particles, respectively, and $Kn = \frac{2\lambda}{d_p}$, the Knudsen number, is the ratio of mean free path of gas molecules to particle diameter.

If mean free path of the fluid particles is comparable to the characteristics dimensions of the flow field domain the assumption of continuum media no longer valid as a consequence Navier–Stokes equations breaks down. In the range of $0.1 < Kn < 10$ the higher order continuum equation should be used. For the range of $0.001 < Kn < 0.10$, the no-slip boundary condition cannot be used and should be replaced with $U_t = \lambda^* \left(\frac{2-\zeta}{\zeta}\right) \frac{\partial u}{\partial z}$, where U_t is the target velocity, ζ is the target momentum accommodation coefficient and λ^* is the mean free path. For $Kn < 0.001$, the no-slip boundary condition is valid, therefore the velocity at the surface is equal to zero. In this study the slip and the no-slip regimes of the Knudsen number that lies in the range $0 < Kn < 0.1$ are considered.

2.1 Boundary conditions

(i) On the surface of the disk ($z = 0$):

$$u = U_t, \quad v = \Omega r + U_t, \quad w = w_w, \quad p = 0, \quad T = T_w, \quad C = C_w = 0 \quad \text{at} \quad z = 0. \tag{2.9}$$

(ii) Matching with the quiescent free stream ($z \to \infty$):

$$u = 0, \quad v = 0, \quad p \to p_\infty, \quad T \to T_\infty, \quad C \to C_\infty \quad \text{as} \quad z \to \infty. \tag{2.10}$$

2.2 Dimensionless governing equations

To obtain the similarity solutions of the governing equations (2.1)–(2.6) along with the boundary conditions (2.9)–(2.10) we introduce the following similarity transformations:

$$\begin{aligned} &\eta = \frac{z}{\delta}, \quad u = \Omega r F(\eta), \quad v = \Omega r G(\eta), \quad w = \frac{\nu}{\delta} H(\eta), \\ &p = -\rho\nu\Omega P(\eta), \quad \theta(\eta) = \frac{T_\infty - T}{T_\infty - T_w}, \quad \phi(\eta) = \frac{C}{C_\infty}, \end{aligned} \tag{2.11}$$

where δ is a scale factor and is a function of time as $\delta = \delta(t)$ which follows from Sattar and Hossain [39] and Rahman et al. [33].

Substituting (2.11) into equations (2.1)–(2.6), we obtain the following differential equations:

$$H' + 2RF = 0, \tag{2.12}$$

$$F'' - HF' - R(F^2 - G^2) + \lambda\eta F' - MF = 0, \tag{2.13}$$

$$G'' - HG' - 2RFG + \lambda\eta G' - MG = 0, \tag{2.14}$$

$$H'' - HH' + RP' + \lambda\eta H' = 0, \tag{2.15}$$

$$\theta'' - PrH\theta' + Pr\lambda\eta\theta' = 0, \tag{2.16}$$

$$\phi'' - ScH\phi' - \kappa ScN_t(1 - N_t\theta)^{-1}(\theta''\phi + \theta'\phi') + Sc\lambda\eta\phi' = 0, \tag{2.17}$$

with the transformed boundary conditions as

$$F = \varepsilon F', \;\; G = 1 + \varepsilon G', \;\; H = w_s, \;\; P = 0, \;\; \theta = 1, \;\; \phi = 0 \quad \text{at} \quad \eta = 0, \tag{2.18}$$

$$F = 0, \;\; G = 0, \;\; \theta = 0, \;\; \phi = 1 \quad \text{as} \quad \eta \to \infty. \tag{2.19}$$

where $\varepsilon = \frac{\lambda}{\delta}(\frac{2-\zeta}{\zeta})$ is the slip parameter and $w_s = \frac{w_w \delta}{\nu}$ represents uniform suction ($w_s < 0$) or injection ($w_s > 0$) velocity at the surface of the disk. The dimensionless parameters introduced in the above equations are: $R = \frac{\Omega\delta^2}{\nu}$ is the rotational parameter, $\lambda = \frac{\delta}{\nu}\frac{\mathrm{d}\delta}{\mathrm{d}t}$ is the unsteadiness parameter, $Pr = \frac{\nu}{\alpha}$ is the Prandtl number, $N_t = \frac{T_\infty - T_w}{T_\infty}$ is the thermophoresis parameter, $Sc = \frac{\nu}{D}$ is the Schmidt number and $M = \frac{\sigma B_0^2 \delta^2}{\rho\nu}$ is the magnetic field parameter. Also in the equations (2.12)–(2.18), primes denote differentiation with respect to the similarity variable η.

It is good to mention that integrating the unsteady relation $\lambda = \frac{\delta}{\nu}\frac{\mathrm{d}\delta}{\mathrm{d}t}$, we obtain $\delta = \sqrt{2\lambda\nu t}$. A choice of $\lambda = 2$ provides $\delta = 2\sqrt{\nu t}$, which exactly coincides with the length scale $\delta(t)$ for various unsteady parallel flow considered by Schlichting [40]. The above-defined characteristic length scale physically related to the boundary layer thickness that can be found in the book by Schlichting [40].

3 Important physical parameters

The quantities of physical interest are the skin-friction coefficient, the Nusselt number, the thermophoretic velocity, the thermophoretic particle deposition velocity and the Stanton number which are obtained from the following expressions. The radial shear stress τ_r and tangential shear stress τ_t are defined by

$$\tau_r = \left[\mu\left(\frac{\partial u}{\partial z} + \frac{\partial w}{\partial r}\right)\right]_{z=0} = \frac{\mu\Omega r}{\delta}F'(\eta), \tag{3.1}$$

$$\tau_t = \left[\mu\left(\frac{\partial v}{\partial z} + \frac{1}{r}\frac{\partial w}{\partial \phi}\right)\right]_{z=0} = \frac{\mu\Omega r}{\delta}G'(\eta). \tag{3.2}$$

Hence the skin-frictions ($Cf = \tau/\rho\Omega^2 r^2$) along the radial and tangential directions are obtained as

$$Cf_r Re = F'(0), \tag{3.3}$$

$$Cf_t Re = G'(0), \tag{3.4}$$

where $Re = \frac{\Omega r \delta}{\nu}$ is the rotational Reynolds number.

The rate of heat transfer from the disk surface to the fluid is computed by the application of Fourier's law as given below

$$q_w = -k\frac{\partial T}{\partial z}_{z=0} = -k\frac{T_\infty - T_w}{\delta}\theta'(0). \tag{3.5}$$

Hence the Nusselt number is obtained as

$$Nu = \frac{\delta q_w}{k(T_\infty - T_w)} = -\theta'(0). \tag{3.6}$$

Thermophoretic velocities at the surface of the disk along the radial and axial directions are evaluated as

$$U_T\,|_{z=0},\ W_T\,|_{z=0} \ = \ -\frac{\nu}{\delta}\frac{\kappa N_t}{1-Nt}\theta'(0). \tag{3.7}$$

Therefore a non-dimensional axial thermophoretic velocity can be written as

$$W_T^* = -\frac{\kappa N_t}{1-Nt}\theta'(0). \tag{3.8}$$

Thermophoretic particle deposition velocity at the surface of the disk is evaluated by

$$V_d = \left(\frac{J_d}{C_\infty}\right)_{z=0} = -\frac{D}{\delta}\phi'(0), \quad \text{where} \quad J_w = -D\left(\frac{\partial C}{\partial z}\right)_{z=0} = -\frac{DC_\infty}{\delta}\phi'(0). \tag{3.9}$$

Therefore non-dimensional thermophoretic particle deposition velocity is evaluated as

$$V_d^* = \frac{V_d\delta}{\nu} = -\frac{1}{Sc}\phi'(0). \tag{3.10}$$

The negative sign in equation (3.10) represents that particle deposition will take place at the surface of the disk from the hotter region to the colder region, *i.e.* from the fluid to the disk along the inward axial direction. Now the local Stanton number is defined as

$$St = -\frac{J_w\delta}{C_\infty\nu}\phi'(0). \tag{3.11}$$

Comparing (3.10) and (3.11) we find that

$$St = -V_d^*. \tag{3.12}$$

4 Method of solutions

The set of equations (2.12)–(2.17) are highly non-linear and coupled and therefore the system cannot be solved analytically. We dropped equation (2.15) from the system as it can be used for calculating pressure once F and H are known from the rest of the equations. Therefore, the equations (2.12)–(2.14) and (2.16)–(2.17) with boundary conditions (2.18)–(2.19) have been solved numerically by using sixth order Runge–Kutta method along with Nachtsheim–Swigert [29] shooting iteration technique (for detailed discussion of the method see Alam et al. [1]) with w_s, R, λ, Pr, κ , N_t, ε, Sc and M as prescribed parameters. A step size of $\Delta\eta = 0.01$ was selected to be satisfactory for a convergence criterion of 10^{-6} in all cases. The value of η_∞ was found to each iteration loop by the statement $\eta_\infty = \eta_\infty + \Delta\eta$. The maximum value of η_∞ to each group of parameters w_s, R, λ, Pr, κ , N_t, ε, Sc and M determined when the value of the unknown boundary conditions at $\eta = 0$ does not change to a successful loop with an error less than 10^{-6}.

4.1 Testing of the code

When $\lambda = 0$ (*i.e.* for steady case), $R = 1$, $M = 0$, $w_s = 0$, $\varepsilon = 0$ and in the absence of heat and mass transfer, the present problem coincides with those of White [46] . To assess the accuracy of the present code, we have calculated the values of F, G and $-H$ for different values of η in the absence of heat and mass transfer.

Table 1 presents a comparison of the data obtained in the present work and those obtained by White [46]. It is clearly observed that very good agreement between the results exists. This lends confidence in the present numerical method.

5 Results and discussion

In order to investigate the effects of the pertinent parameters such as suction/injection parameter w_s, slip parameter ε, magnetic field parameter M, rotational parameter R, unsteadiness parameter λ,

Prandtl number Pr, thermophoretic coefficient κ, thermophoresis parameter N_t and Schmidt number Sc on the flow, heat and mass transfer characteristics are presented graphically as well as in tabular form. For the present investigation we considered our working fluid as air ($Pr = 0.71$) and the species is carbon dioxide ($Sc = 0.94$). The default values of the other parameters throughout the simulation are considered as $\varepsilon = 1.0$, $w_s = 0.6$, $R = 1.0$, $\lambda = 0.5$, $N_t = 0.5$, $\kappa = 0.5$ and $M = 0.5$ unless otherwise specified.

The effects of the suction (or injection) parameter (w_s) on the radial, tangential, and axial velocity profile are shown in Figs. 2(a)–(e) respectively. From Figs. 2(a)–(b) we see that radial and tangential velocity profile decrease very rapidly as the suction velocity ($w_s < 0$) increases. The maximum of the radial velocity profiles moves toward the surface of the disk. It is also apparent that the thickness of the boundary layer decreases as the suction velocity increases. In Fig. 2(c) we observe that for strong suction, inward axial velocity is nearly constant. The effect of the suction parameter on the thermal boundary layer is found to be similar to those of the radial and tangential velocity boundary layers, which is shown in Fig. 2(d). The effects of suction parameter on the concentration field are displayed in Fig. 2(e), which shows that the concentration increases as the suction parameter w_s increases. An opposite effect is found for the case of fluid injection ($w_s > 0$).

The effect of the slip parameter ε on the non-dimensional velocity, temperature and concentration profiles are presented. From Fig. 3(a) we see that boundary layer decreases very rapidly with the increase of the slip parameter. Fig. 3(b) indicates that for large values of ε, *i.e.* $\varepsilon \to \infty$, the rotating disk does not cause rotation of the fluid particles. Because in this range of ε the flow becomes entirely potential, there will be no motion in the fluid. This can be further explained as follows: the centrifugal force acting on the rotating disk will throw out the fluid that sticks to it. On the other hand the flow in the axial direction will come forward to compensate for this thrown fluid. But increasing the slip on the surface of the disk reduces the amount of fluid that can stick on it; as a consequence the efficiency of the rotating disk is reduced substantially and is unable to transfer its circumferential momentum to the fluid particles. A reduction in the circumferential velocity results in a reduction in the centrifugal force which in turn decreases the inward axial velocity substantially as can be seen from Fig. 3(c). From Fig. 3(d) it is noticed that thermal boundary layer increases as slip parameter increases. Fig. 3(e) shows a decreasing effect of ε on the concentration boundary layer.

In Figs. 4(a)–(e), the influence of the unsteadiness parameter λ on the dimensionless radial, tangential, inward axial velocity, temperature and concentration profiles across the boundary layer have been displayed, respectively. From these figures we observe that the radial, tangential, inward axial velocity and temperature profiles decrease whereas concentration profiles increases with an increasing values of the unsteadiness parameter.

The effects of rotational parameter R on the dimensionless radial, tangential, inward axial velocity, temperature and concentration profiles have been shown in Figs. 5(a)–(e) respectively. From these figures we observe that the radial, inward axial velocity and concentration profiles increase whereas both the tangential velocity and temperature profiles decrease with increasing values of the rotational parameter.

Figs. 6(a)–(e) show the effect of the magnetic field on the dimensionless radial, tangential, inward axial velocity, temperature and concentration profiles. Radial, tangential and axial velocity decelerate as M increases as shown in Figs. 6(a), 6(b) and 6(c). A drag-like force called Lorentz force is generally created due to the introduction of the magnetic field which has the tendency to decelerate the flow around the disk at the expense of increasing its temperature as shown in Fig. 6(d). It can further be mentioned that the thicknesses of the concentration boundary layer decreases with

the increase of the strength of the applied magnetic field which is shown in Fig. 6(e).

Figs. 7(a)–(b) show typical concentration profiles across the boundary layer for various values of the Schmidt number Sc. An increasing Schmidt number thickens the concentration boundary layer. Fig. 7(a) plotted for some values of Sc, shows that concentration profile increases with the increase of the Schmidt number. Fig. 7(b) plotted for large values of Sc, shows that increase of these profiles is very steep for large Schmidt numbers. From the physical point of view, for smaller values of the Schmidt number, Brownian diffusion effect is more important as compared to the convection effect. However, for a large value of Sc the diffusion effect is minimal as compared to the convection effect and, therefore, the effect of thermophoresis alters the concentration boundary layer significantly.

The effect of the thermophoretic coefficient κ on the concentration profiles is depicted in Fig. 7(c). The effect of increasing the thermophoretic coefficient κ is to decrease the slope of the concentration profiles except very close to the surface of the disk ($\eta < 1.0$). This is due to the fact that thermophoresis plays a suction-like effect on particles for a cold surface. This phenomenon is consistent with the works of Rahman and Postelnicu [34]. In order to examine the effect of thermophoresis on particle deposition onto a rotating disk surface, the concentration profiles are displayed in Fig. 7(d), for thermophoresis parameter N_t. According to the definition of the relative temperature difference parameter, $N_t < 1$ always, this is positive for a cooled surface and negative for a heated surface. From this figure it is clear that the concentration profiles are decreased when temperature ratios are increased; this is because when large temperature difference exists, then the thermophoretic force drives more particles closer to the disk so to decrease the concentration somewhere far from the cold surface.

It is noted from Table 2 that the values of the tangential skin friction and the rate of heat transfer coefficients as well as deposition flux decrease and radial skin friction increases for increasing values of the injection velocity. It is also noted from this table that increasing the suction velocity leads to decrease in the radial skin friction coefficient and while its effect is to increase the tangential skin friction coefficient and the rate of heat transfer coefficient as well as deposition flux. Table 2 also shows that skin friction along the radial and tangential directions; the rate of heat transfer and deposition flux increase with the increasing values of rotational parameter R. From Table 2 we further see that radial skin friction decreases whereas tangential skin friction and the rate of heat transfer as well as deposition flux increase with the increasing values of the unsteadiness parameter λ. It is also seen that an increase in M leads to an increase in tangential skin friction whereas its influence is to decrease the radial skin friction, rate of heat transfer and deposition flux. From this table we noted that skin friction in both directions decreases with the increase of the slip parameter. The largest skin friction is found for the case of no-slip at the surface. On the other hand the rate of heat transfer increases with the increase of slip parameter within the range $0 \leq \varepsilon \leq 0.5$. Outside of this range of the heat transfer and deposition flux decrease with the further increase of the slip parameter. Thus, the rate of heat transfer can be strongly controlled by controlling the slip on the disk.

From Table 3 we see that the non-dimensional axial thermophoretic velocity W_T^* increases with the increase of the thermophoretic coefficient κ as well as thermophoresis parameter N_t. Finally, Table 4 shows the variations of thermophoretic deposition velocity for different values of the Schmidt number Sc and thermophoretic coefficient κ. From this table it is also clear that the effect of increasing Schmidt number lead asymptotically to a zero thermophoretic deposition velocity. This is in agreement with the physical explanations, based on the fact that the Schmidt number is the ratio of momentum diffusivity (viscosity) to mass diffusivity. This table confirms that the thermophoretic deposition velocity decreases as the thermophoretic coefficient κ increases.

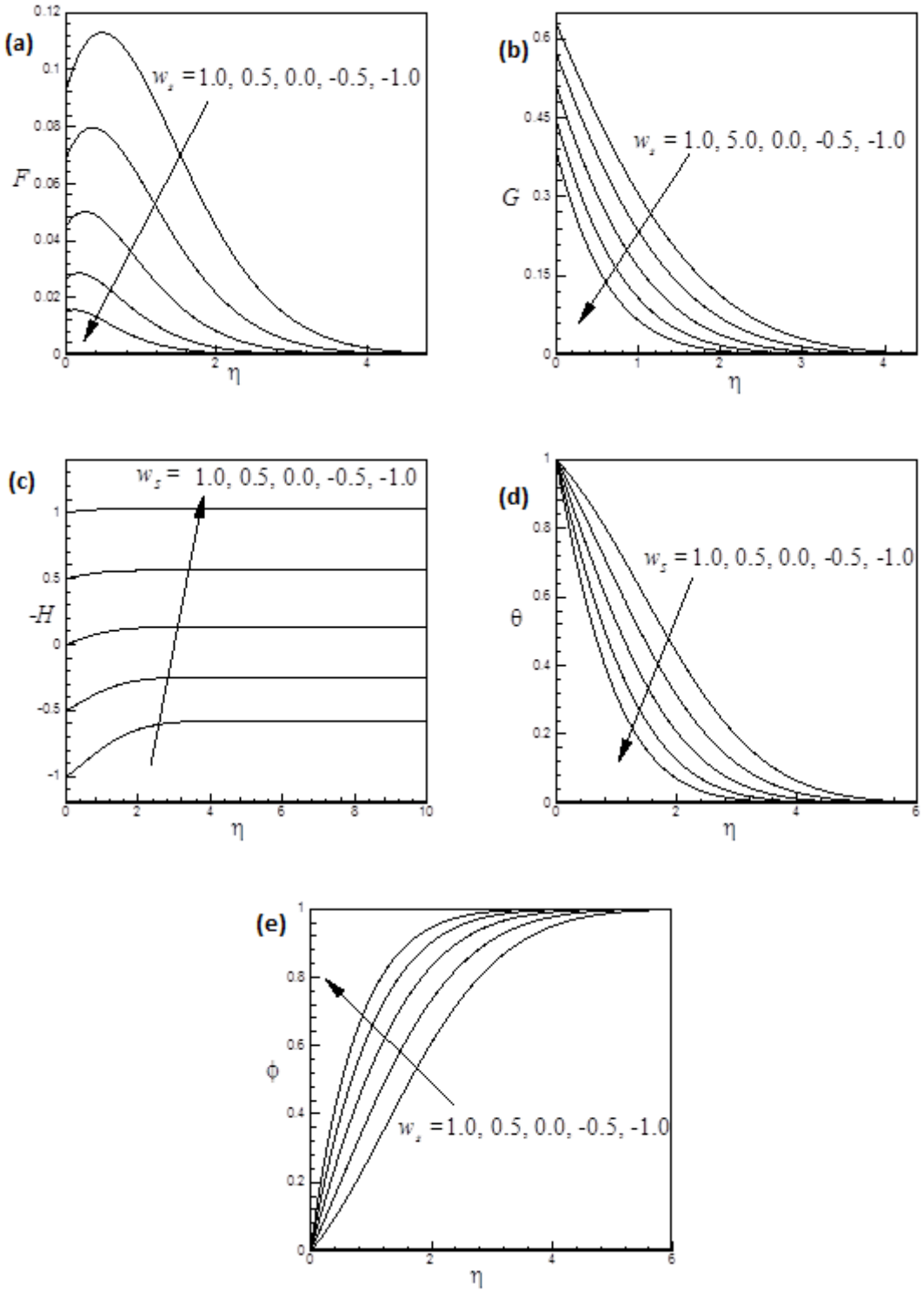

Figure 2: Variation of (a) radial velocity, (b) tangential velocity, (c) axial velocity, (d) temperature profiles and (e) concentration profiles for several values of w_s.

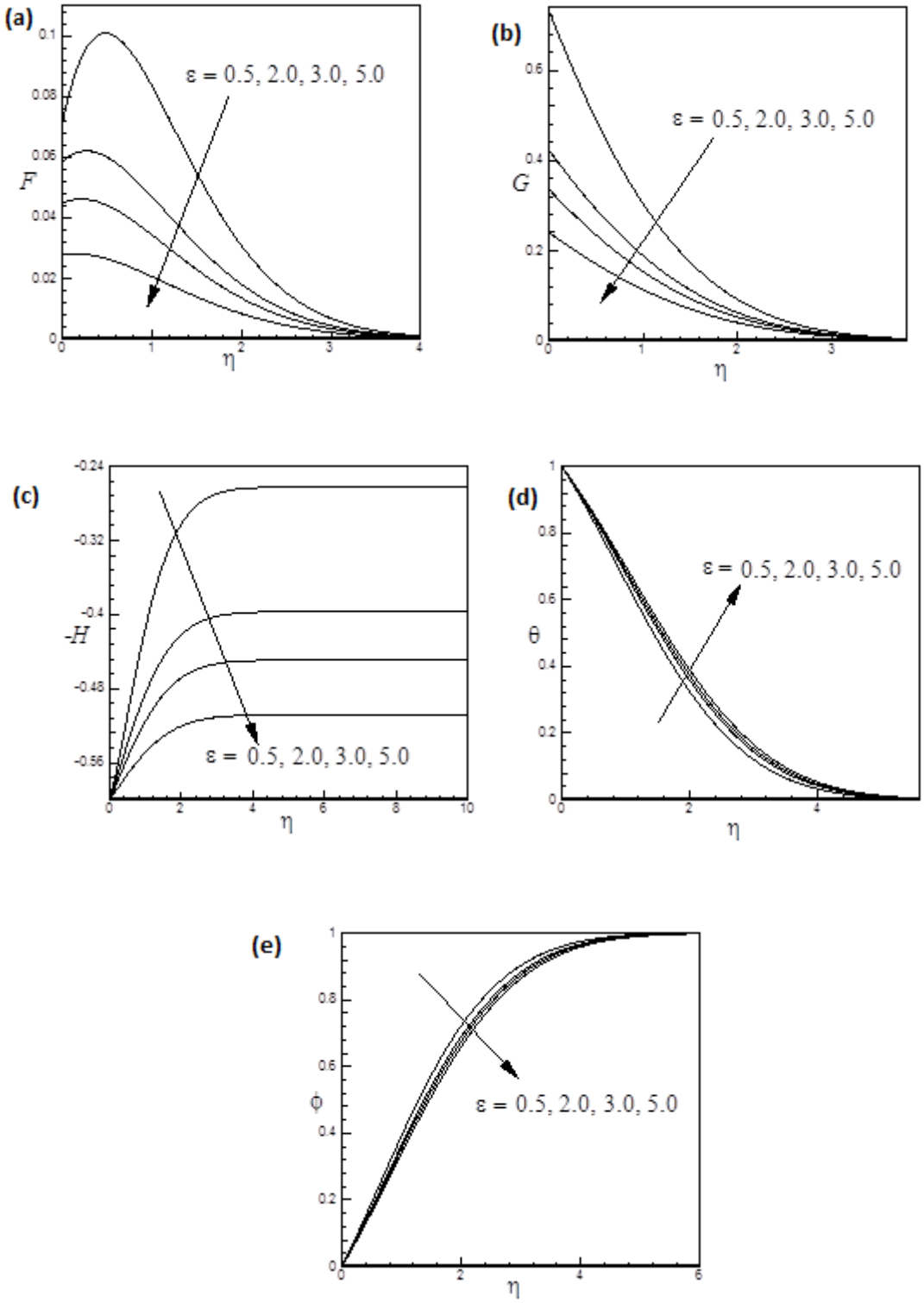

Figure 3: Variation of (a) radial velocity, (b) tangential velocity, (c) axial velocity, (d) temperature profiles and (e) concentration profiles for several values of ε.

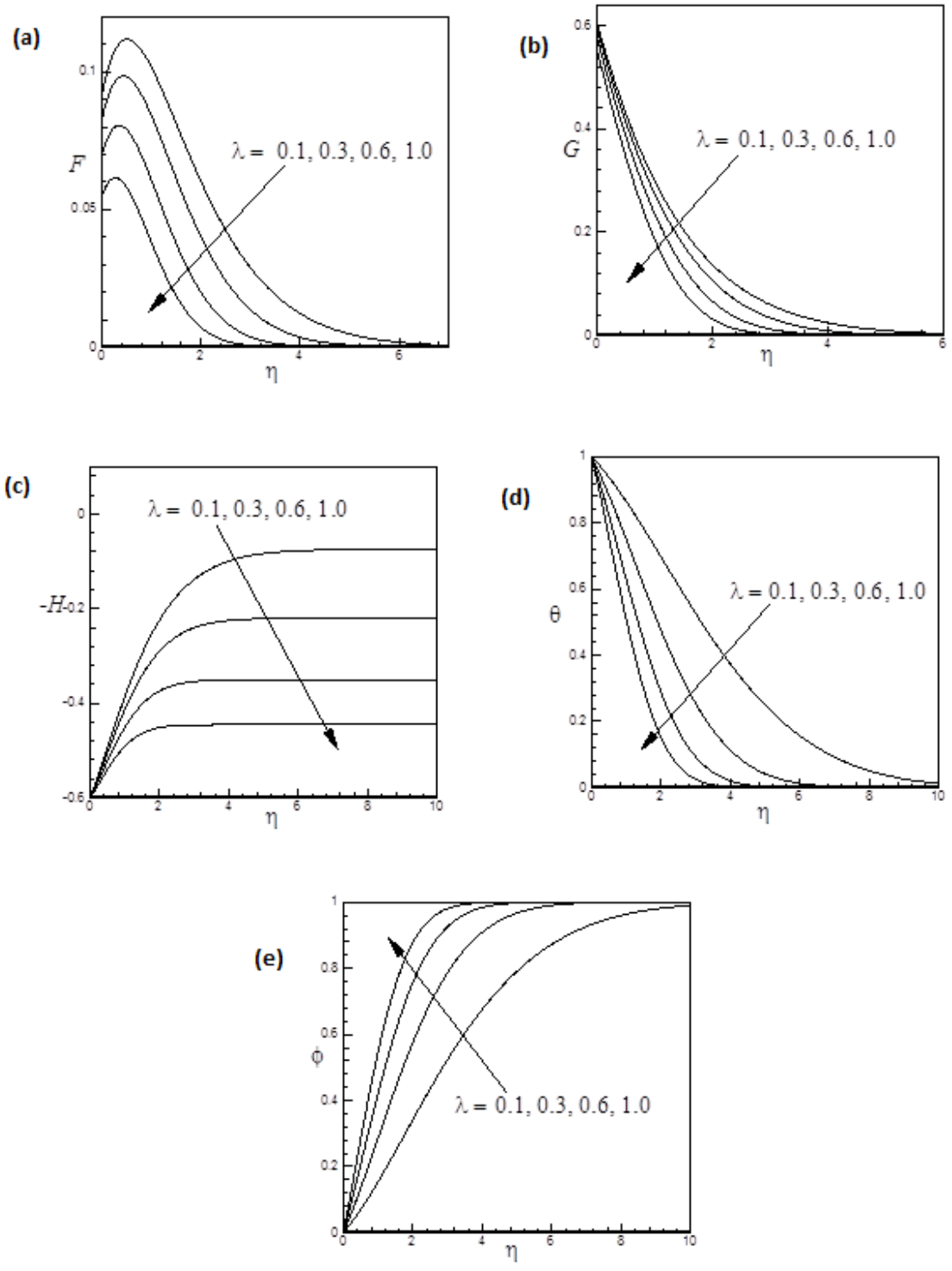

Figure 4: Variation of (a) radial velocity, (b) tangential velocity, (c) axial velocity, (d) temperature profile and (e) concentration profile for several values of λ.

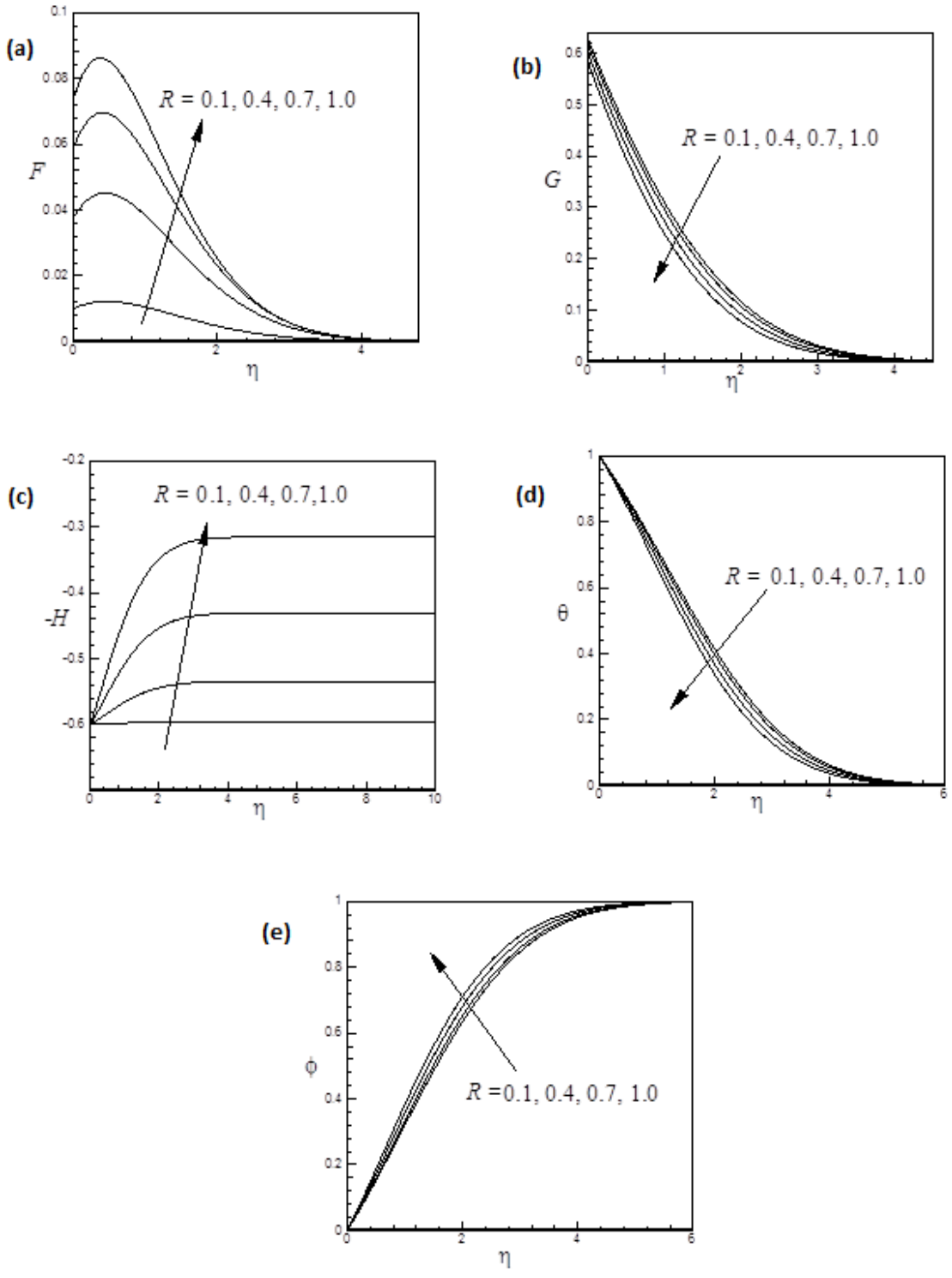

Figure 5: Variation of (a) radial velocity,(b) tangential velocity, (c) axial velocity,(d) temperature profiles and (e) concentration profiles for several values of R.

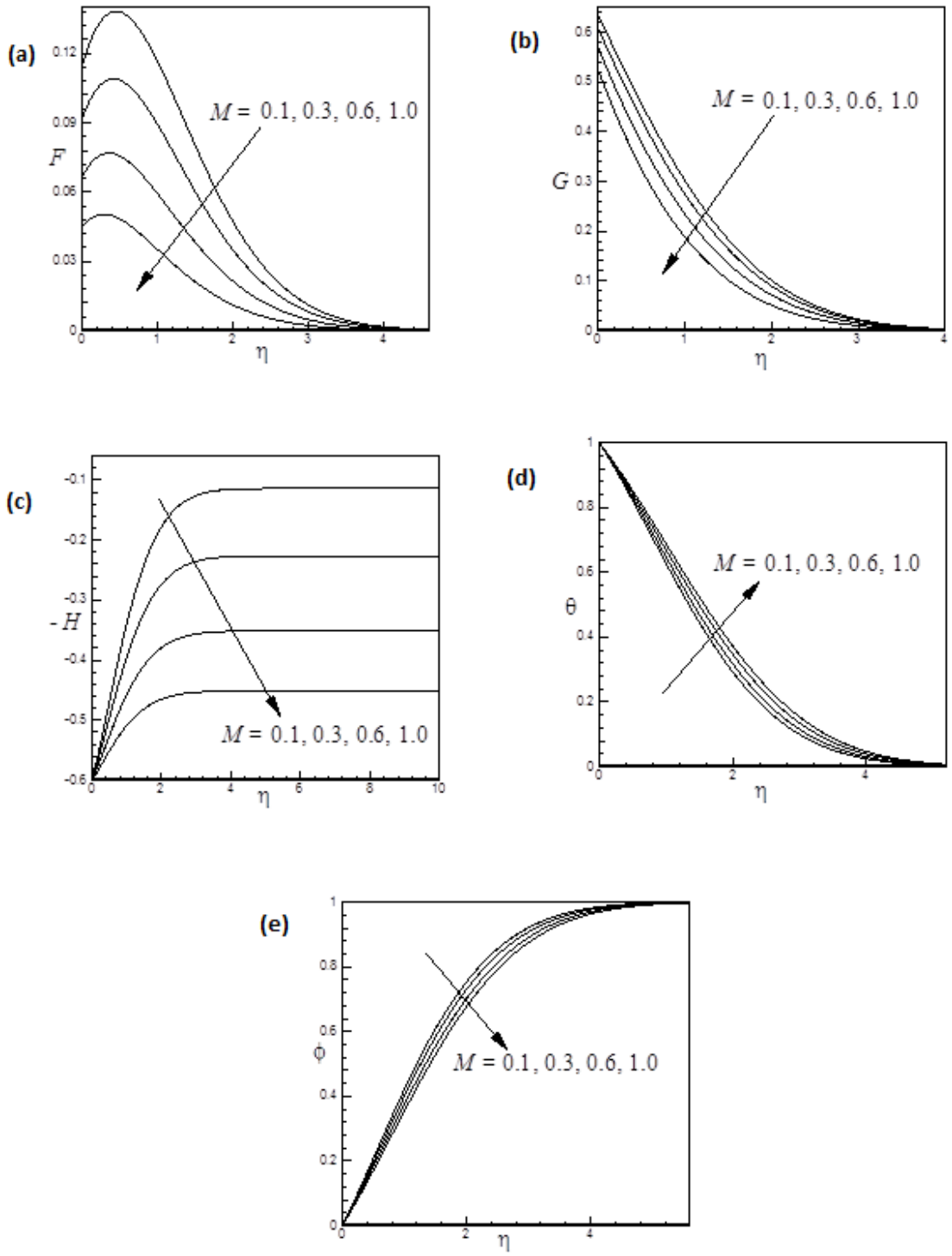

Figure 6: Variation of (a) radial velocity,(b) tangential velocity, (c) axial velocity,(d) temperature profiles and (e) concentration profiles for several values of M.

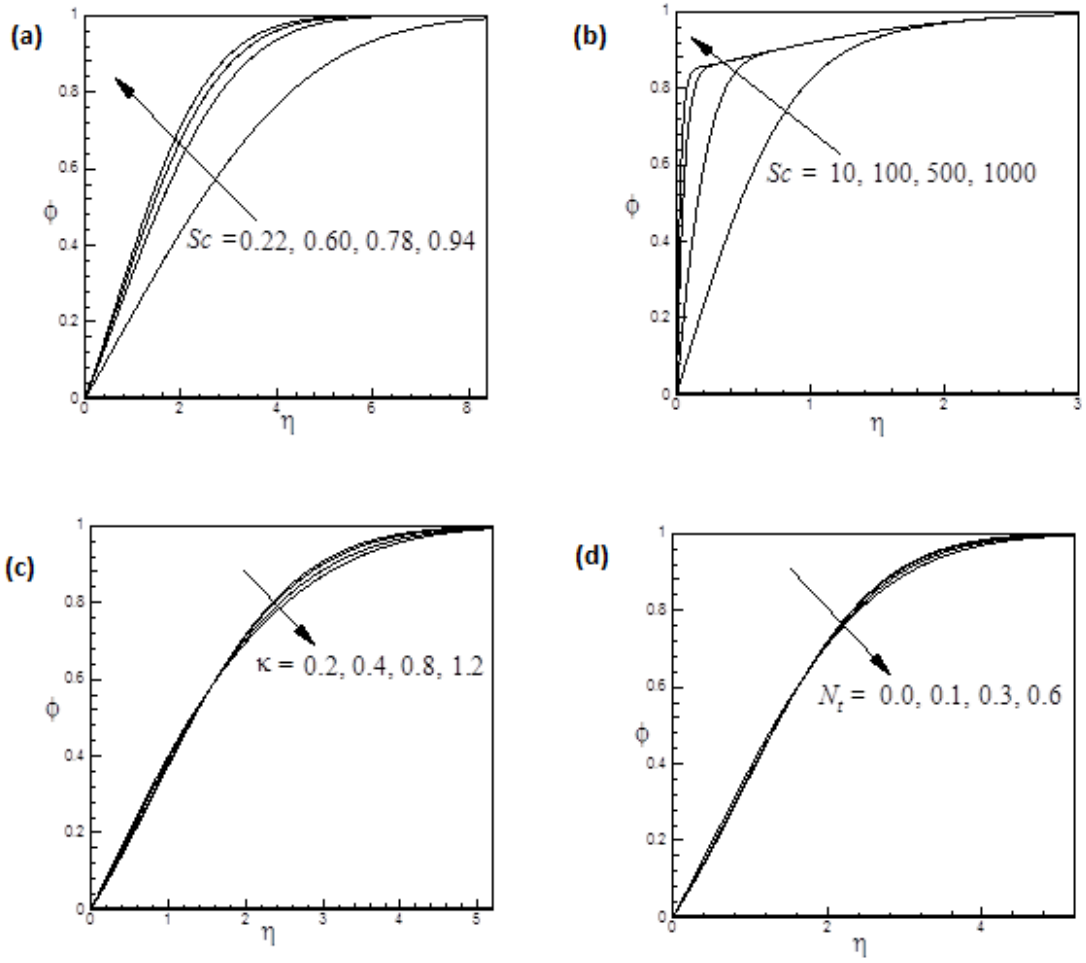

Figure 7: Concentration variation for different values of (a)$Sc < 1$, (b)$Sc >> 1$, (c) κ, and (d) N_t.

Table 1: Numerical values of $F(\eta)$, $G(\eta)$ and $-H(\eta)$ without heat and mass transfer and for $\lambda = M = w_s = \varepsilon = 0$ and $R = 1$.

η	$F(\eta)$		$G(\eta)$		$-H(\eta)$	
	present work	White [46]	present work	White [46]	present work	White [46]
0.0	0.00000000	0.0000	1.00000000	1.0000	0.00000000	0.0000
1.0	0.18002352	0.1801	0.47666771	0.4766	0.26534785	0.2655
2.0	0.11854839	0.1188	0.20329060	0.2034	0.57264331	0.5732
3.0	0.05655563	0.0581	0.08423853	0.0845	0.74391508	0.7452
4.0	0.02507942	0.0256	0.03440941	0.0349	0.82266964	0.8249
5.0	0.01022057	0.0108	0.01369313	0.0144	0.85594800	0.8594

Table 2: Variation of $F'(0)$, $-G'(0)$, $-\theta'(0)$ and $-\phi'(0)$ for different values of w_s, R, λ, M and ε at $Pr = 0.71$, $\kappa = 0.5$, $N_t = 0.5$ and $Sc = 0.94$.

w_s	R	λ	M	ε	$F'(0)$	$-G'(0)$	$-\theta'(0)$	$-\phi'(0)$
1.0	1.0	0.5	0.5	1.0	0.0927266	0.3721130	0.1914136	0.2067976
0.5	1.0	0.5	0.5	1.0	0.0687145	0.4274587	0.3251592	0.3862128
0.0	1.0	0.5	0.5	1.0	0.0450152	0.4895662	0.5886159	0.6403698
-0.5	1.0	0.5	0.5	1.0	0.0265266	0.5536815	0.7402647	0.9638555
-1.0	1.0	0.5	0.5	1.0	0.0148325	0.6131033	1.0106508	1.3407542
0.6	0.2	0.5	0.5	1.0	0.0198669	0.3744116	0.2445934	0.2812372
0.6	0.4	0.5	0.5	1.0	0.0376886	0.3818944	0.2530752	0.2919466
0.6	0.6	0.5	0.5	1.0	0.0524955	0.3922625	0.2652003	0.3072754
0.6	0.8	0.5	0.5	1.0	0.0643293	0.4038964	0.2794172	0.3252551
0.6	1.0	0.5	0.5	1.0	0.0736667	0.4157733	0.2944743	0.3443481
0.6	1.0	0.1	0.5	1.0	0.0915046	0.3948652	0.1139683	0.1256954
0.6	1.0	0.3	0.5	1.0	0.0825447	0.4047808	0.2150747	0.2470199
0.6	1.0	0.5	0.5	1.0	0.0736667	0.4157733	0.2944743	0.3443481
0.6	1.0	0.7	0.5	1.0	0.0653891	0.4275072	0.3638482	0.4300710
0.6	1.0	1.0	0.5	1.0	0.0545749	0.4456690	0.4564223	0.5450685
0.6	1.0	0.5	0.5	1.0	0.0736667	0.4157733	0.2944743	0.3443481
0.6	1.0	0.5	1.5	1.0	0.0292621	0.5177313	0.26885316	0.2994761
0.6	1.0	0.5	2.5	1.0	0.0153430	0.5812493	0.2492675	0.2873027
0.6	1.0	0.5	3.0	1.0	0.0118888	0.6044182	0.24714064	0.28458906
0.6	1.0	0.5	4.0	1.0	0.0077865	0.6404763	0.24481106	0.28160777
0.6	1.0	0.5	0.5	0.0	0.3553806	0.6985804	0.2986664	0.3484625
0.6	1.0	0.5	0.5	0.5	0.1418910	0.5330671	0.3032187	0.3551829
0.6	1.0	0.5	0.5	1.0	0.0736667	0.4157733	0.2944743	0.3443481
0.6	1.0	0.5	0.5	2.0	0.0291623	0.2880587	0.2794093	0.3253503
0.6	1.0	0.5	0.5	5.0	0.0055400	0.1519075	0.2584244	0.2987912
0.6	1.0	0.5	0.5	8.0	0.0019516	0.1038555	0.2508964	0.2892476

Table 3: Variation of non-dimensional axial thermophoretic velocity W_T^* for different values of thermophoretic coefficient κ, and thermophoresis parameter N_t.

κ	N_t	$W_T^* = -\frac{\kappa N_t}{(1-N_t)}\theta'(0)$
0.2		0.05088
0.4		0.11779
0.8	0.50	0.23558
1.0		0.29447
1.2		0.35337
	0.0	0.0000
	0.1	0.01636
	0.3	0.06310
0.50	0.6	0.22086
	0.8	0.59885
	0.9	1.32514

Table 4: Variation of non-dimensional thermophoretic deposition velocity V_d^* for different values of Schmidt number Sc, and thermophoretic coefficient κ.

Sc	κ	$St = -V_d^*$
0.22		2.6535056
0.60		1.0274275
0.78	0.5	0.6936924
0.94		0.6860257
100		0.0416088
1000		0.0297816
2000		0.0194139
	0.2	0.3424810
	0.4	0.3549821
	0.8	0.3908922
0.94	1.0	0.4076531
	1.2	0.4467840

6 Conclusions

In this paper, we have studied the effects of thermophoresis on unsteady hydromagnetic forced convective heat and mass transfer flow of a viscous incompressible fluid over a cold rapidly rotating disk in the presence of partial slip at its surface under the action of an applied magnetic field. Using similarity transformations, the governing non-linear partial differential equations have been transferred into a system of ordinary differential equations which are solved numerically by applying

Nachtsheim–Swigert shooting iteration technique along with sixth-order Runge–Kutta integration scheme. Comparison with previously published work for steady case of the problem was performed and the results are found to be in excellent agreement. From the present numerical investigations the following major conclusions may be drawn.

1. Radial, tangential, and temperature profiles decrease whereas both inward axial velocity and concentration profiles increase with the increase of the suction velocity. An opposite trend is also observed for the case of injection. Suction and injection stabilizes the growth of the boundary layer.

2. Slip parameter significantly controls the flow, heat and mass transfer characteristics.

3. Magnetic field significantly controls the skin friction coefficient along tangential and radial directions. The rate of heat transfer and deposition flux reduces due to an intensification of the applied magnetic field strength.

4. Radial, inward axial velocity and concentration profiles increase whereas both the tangential velocity and temperature profiles decrease with increasing values of the rotational parameter.

5. Radial, tangential, inward axial velocity and temperature profiles decrease whereas concentration profiles increase with the increasing values of the unsteadiness parameter.

6. Radial, tangential, and axial velocity decelerate as magnetic field parameter increases. It can be also noticed that the temperature profile increases whereas concentration profile decreases with the increase of the magnetic field parameter.

7. Concentration profiles decrease with the increase of thermophoretic coefficient and the thermophoresis parameter. On the other hand it increases with the increase of the Schmidt number.

8. Axial thermophoretic velocity increases linearly with the increase of the thermophoretic coefficient and thermophoresis parameter.

9. Inward axial thermophoretic particle deposition velocity decreases with the increase of the Schmidt number. On the other hand, it increases with the increasing values of the thermophoretic coefficient.

   Nanofluids are a new class of fluids which can be used for various purposes specially for solar collectors to improve the efficiency of the collector. The interdisciplinary nature of nanofluids research presents a great opportunity for exploration and discovery at the frontiers of nanotechnology. An investigation is under way exploring the heat transfer augmentation considering nanofluid in the present model.

Nomenclature

B_0	Applied magnetic field	T_w	Temperature at the surface of the disk
Cf	Skin friction coefficient	T_∞	Temperature of the ambient fluid
c_p	Specific heat at constant pressure	U_t	Target velocity
C	Concentration within the boundary layer	u, v, w	Velocities along radial, tangential and axial direction respectively
C_w	Concentration at the surface of the disk	V_d^*	Thermophoretic particle deposition velocity
C_∞	Concentration of the ambient fluid	W_T^*	Axial thermophoretic velocity
D	Molecular diffusivity	w_w/w_s	Dimensional/non dimensional suction and injection velocity
F	Dimensionless radial velocity	z	Axial coordinate
G	Dimensionless tangential velocity		**Greek symbols**
H	Dimensionless axial velocity	ρ	Density of the fluid
k	Thermal conductivity of the fluid	μ	Coefficient of dynamic viscosity
K_n	Knudsen number	ν	Kinematic viscosity
M	Magnetic field parameter	κ	Thermophoretic coefficient
N_t	Thermophoresis parameter	α	Thermal diffusivity
Nu	Nusselt number	η	Similarity variable
p_∞	Pressure of the ambient fluid	δ	Time dependent length scale
Pr	Prandtl number	λ	Unsteadiness parameter
q_w	Surface heat flux	λ^*	Mean free path
R	Rotational parameter	ϕ	Dimensionless concentration
Re	Rotational Reynolds number	φ	Cylindrical tangential coordinate
r	Cylindrical radial coordinate	τ_r	Radial shear stress
Sc	Schmidt number	τ_t	Tangential shear stress
St	Stanton number	θ	Dimensionless temperature
t	Time	Ω	Angular velocity
T	Temperature within the boundary layer	ε	Slip parameter

Acknowledgements

M. M. Rahman is grateful to The Research Council (TRC) of Oman for funding under the Open Research Grant Program: ORG/SQU/CBS/14/007 and College of Science, Sultan Qaboos University for the grant IG/SCI/DOMS/16/15.

References

[1] M. S. Alam, M. M. Rahman, M. A. Samad, *Numerical study of the combined free-forced convection and mass transfer flow past a vertical porous plate in a porous medium with heat generation and thermal diffusion*, Nonlinear Analysis: Modelling and Control **11** (2006), pp. 331–343.

[2] M. S. Alam, M. M. Rahman, M. A. Sattar, *On the effectiveness of viscous dissipation and Joule heating on steady magnetohydrodynamic heat and mass transfer flow over an inclined radiate isothermal permeable surface in the presence of thermophoresis*, Communications in Nonlinear Science and Numerical Simulations **14** (2009), pp. 2132–2143.

[3] A. Arikoglu, I. Ozkol, *On the MHD and slip flow over a rotating disk with heat transfer*, International Journal of Numerical Methods for Heat and Fluid Flow **28** (2006), pp. 172–184.

[4] H. A. Attia, *Steady flow over a rotating disk in porous medium with heat transfer*, Nonlinear Analysis: Modeling and Control **14** (2009), pp. 21–26

[5] A. Y. Bakier, M. A. Mansour, *Combined of magnetic field and thermophoresis particle deposition in free convection boundary layer from a vertical flat plate embedded in a porous medium*, Thermal Science **11** (2007), pp. 65–74.

[6] G. K. Batchelor, C. Shen, *Thermophoretic deposition of particles in gas flowing over cold surface*, Journal of Colloid and Interface Science **107** (1985), pp. 21–37.

[7] U. T. Bödewadt, *Die Drehströmung über festem Grunde*, Zeitschrift für angewandte Mathematik und Mechanik **20** (1940), pp. 241–253.

[8] A. J. Chamkha, C. Issa, *Effects of heat generation/absorption and thermophoresis on hydromagnetic flow with heat and mass transfer over a flat surface*, International Journal of Numerical Methods for Heat and Fluid Flow **10** (2000), pp. 432–448.

[9] A. J. Chamkha, M. Jaradat, I. Pop, *Thermophoresis free convection from a vertical cylinder embedded in a porous medium*, International Journal of Applied Mechanics and Engineering **9** (2004), pp. 471–481.

[10] M. C. Chiou, J. W. Cleaver, *Effects of thermophoresis on sub-micron particle deposition from a laminar forced convection boundary layer flow on to an isothermal cylinder*, Journal of Aerosol Science **27** (1996), pp. 1155–1167.

[11] M. C. Chiou, *Effects of thermophoresis on sub-micron particle deposition from a laminar forced laminar boundary layer flow on to a isothermal moving plate*, Acta Mechanica **129** (1998), pp. 219–229.

[12] W. G. Cochran, *The flow due to a rotating disk*, Cambridge Philosophical Society Proceedings **30** (1934), pp. 365–375.

[13] R. A. Damesh, M. S. Tahat, A. C. Benim, *Non-similar solutions of magnetohydrodynamic and thermophoresis particle deposition on mixed convection problem in porous media along a vertical surface with variable wall temperature*, Progress in Computational Fluid Dynamics **9** (2009), pp. 58–65.

[14] H. M. Duwairi, R. A. Damesh, *Effects of thermophoresis particle deposition on mixed convection from a vertical surface embedded in saturated porous medium*, International Journal of Numerical Methods for Heat and Fluid Flow **18** (2008), pp. 202–216.

[15] M. Epstein, G. M. Hauser, R. E. Henry, *Thermophoretic deposition of particles in natural convection from a vertical plate*, Journal of Heat Transfer **107** (1985), pp. 272–276.

[16] B. Ganga, S. M. Y. Ansari, N. V. Ganesh, A. K. A. Hakeem, *MHD radiative boundary layer flow of nanofluid past a vertical plate with internal heat generation/absorption, viscous and ohmic dissipation effects*, Journal of the Nigerian Mathematical Society **34** (2015), pp. 181–194.

[17] V. K. Garg, S. Jayaraj, *Thermophoresis of aerosol particles in laminar flow over inclined plates*, International Journal of Heat and Mass Transfer **31** (1988), pp. 875–890.

[18] V. K. Garg, S. Jayaraj, *Thermophoretic deposition over a cylinder*, International Journal of Engineering Fluid Mechanics **3** (1990), pp. 175–196.

[19] S. L. Goren, *Thermophoresis of aerosol particles in laminar boundary layer on flat plate*, Journal of Colloid and Interface Science **61** (1977), pp. 77–85.

[20] A. K. A. Hakeem, N. V. Ganesh, B. Ganga, *Magnetic field effect on second order slip flow of nanofluid over a stretching/shrinking sheet with thermal radiation effect*, Journal of Magnetism and Magnetic Materials **381** (2015), pp. 243–257.

[21] A. K. A. Hakeem, P. Renuka, N. V. Ganesh, R. Kalaivanan, B. Ganga, *Influence of inclined Lorentz forces on boundary layer flow of Casson fluid over an impermeable stretching sheet with heat transfer*, Journal of Magnetism and Magnetic Materials **401** (2016), pp. 354–361.

[22] S. Jayaraj, K. K. Dinesh, K. L. Pillai, *Thermophoresis in natural convection with variable properties*, Heat and Mass Transfer **34** (1999), pp. 469–475.

[23] G. Jia, J. W. Cipolla, Y. Yener, *Thermophoresis of a radiating aerosol in laminar boundary layer flow*, Journal of Thermophysics Heat Transfer **6** (1992), pp. 476–482.

[24] T. V. Kármán, *Über laminare and turbulente Reibung*, Zeitschrift für angewandte Mathematik und Mechanik **1** (1921), pp. 233–252.

[25] K. A. Maleque, M. A. Sattar, *Steady laminar convective flow with variable properties due to a porous rotating disk*, Journal of Heat Transfer **127** (2005), pp. 1406–1409.

[26] M. Miklavčič, C. Y. Wang, *The flow due to a rough rotating disk*, Zeitschrift für angewandte Mathematik und Physik **55** (2004), pp. 235–246.

[27] A. F. Mills, X. Hang, F. Ayazi, *The effect of wall suction and thermophoresis on aerosol particle deposition from a laminar boundary layer on a flat plate*, International Journal of Heat and Mass Transfer **27** (1984), pp. 1110–1114.

[28] K. Millsaps, K. Pohlhausen, *Heat transfer by laminar flow from a rotating plate*, Journal of Aeronautical Science **19** (1952), pp. 120–126.

[29] P. R. Nachtsheim, P. Swigert, *Satisfaction of the asymptotic boundary conditions in numerical solution of the system of nonlinear equations of boundary layer type*, NASA TND-3004, 1965.

[30] E. Osalusi, J. Side, R. Harris, *Thermal-diffusion and diffusion-thermo effects on combined heat and mass transfer of a steady MHD convective and slip flow due to a rotating disk with viscous dissipation and Ohmic heating*, International Communications in Heat and Mass Transfer **35** (2008), pp. 908–915.

[31] A. Postelnicu, *Effects of thermophoresis particle deposition in free convection boundary layer from a horizontal flat plate embedded in a porous medium*, International Journal of Heat and Mass Transfer **50** (2007), pp. 2981–2985.

[32] A. Postelnicu, *Thermophoresis Particle deposition in natural convection over inclined surfaces in porous media*, International Journal of Heat and Mass Transfer **55** (2012), pp. 2087–2094.

[33] ATM. M. Rahman, M. S. Alam, M. K. Chowdhury, *Thermophoresis particle deposition on unsteady two dimensional forced convective heat and mass transfer flow along a wedge with variable viscosity and variable Prandtl number*, International Communications in Heat and Mass Transfer **39** (2012), pp. 541–550.

[34] M. M. Rahman, A. Postelnicu, *Effects of thermophoresis on the forced convective laminar flow of a viscous incompressible fluid over a rotating disk*, Mechanics Research Communication **37** (2010), pp. 598–603.

[35] M. M. Rahman, I. A. Eltayeb, *Radiative heat transfer in a hydromagnetic nanofluid past a non-linear stretching surface with convective boundary condition*, Meccanica **48** (2013), pp. 601–615.

[36] M. M. Rahman, M. A. Sattar, *MHD free convection and mass transfer flow with oscillatory plate velocity and constant heat source in a rotating frame of reference*, Dhaka University Journal of Science **47** (1999), pp. 63–73.

[37] M. M. Rahman, *Convective hydromagentic slip flow with variable properties due to a porous rotating disk*, Sultan Qaboos University Journal for Science **15** (2010), pp. 55–79.

[38] M. M. Rahman, *Thermophoretic deposition of nanoparticles due to a permeable rotating disk*: *effects of partial slip, magnetic field, thermal radiation, thermal-diffusion and diffusion-thermo*, World Academy of Science, Engineering and Technology **77** (2013), pp. 5–20.

[39] M. A. Sattar, M. M. Hossain, *Unsteady hydromagnetic free convection flow with hall current and mass transfer along an accelerated porous plate with time dependent temperature and concentration*, Canadian Journal of Physics **70** (1992), pp. 369–374.

[40] H. Schlichting, *Boundary layer theory*, McGraw Hill, 1968.

[41] M. A. Seddeek, *Influence of viscous dissipation and thermophoresis on Darcy–Forchheimer mixed convection in a fluid saturated porous media*, Journal of Colloid Interface and Science **293** (2006), pp. 137–142.

[42] E. M. Sparrow, G. S. Beavers, L. Y. Hung, *Flow about a porous-surface rotating disk*, International Journal of Heat and Mass Transfer **14** (1971), pp. 993–996.

[43] L. Talbot, R. K. Cheng, R. W. Schefer, D. R. Willis, *Thermophoresis of particles in a heated boundary layer*, Journal of Fluid Mechanics **101** (1980), pp. 737–758.

[44] R. Tsai, *A simple approach of evaluating the effect of wall suction and thermophoresis on aerosol particle deposition from a laminar flow over a flat plate*, International Communications in Heat and Mass Transfer **26** (1999), pp. 249-257.

[45] C. Wagner, *Heat transfer from a rotating disk to ambient air*, Journal of Applied Physics **19** (1948), pp. 837–839.

[46] F. M. White, *Viscous fluid flows*, McGraw-Hill, Inc., New York, 1991.

[47] J. Zueco, V. Rubio, *Network method to study magnetohydrodynamic flow and heat transfer about rotating disk*, Engineering Applied Computational Fluid Dynamics **6** (2012), pp. 336–345.